Int. J. Solids Structures Vol. 28, No. 7, pp. 897–915, 1991
Printed in Great Britain.

0020–7683/91 $3.00 + .00

A BOUNDARY ELEMENT METHOD FOR AXISYMMETRIC SOIL CONSOLIDATION

G. F. DARGUSH and P. K. BANERJEE
Department of Civil Engineering, State University of New York at Buffalo, Buffalo, NY 14260, U.S.A.

(*Received* 6 *September* 1990)

Abstract—The development of a time domain boundary element method for axisymmetric quasi-static poroelasticity is discussed. This new formulation, for the complete Biot consolidation theory, has the distinct advantage of being written exclusively in terms of boundary variables. Thus, no volume discretization is required, and the approach is ideally suited for geotechnical problems involving media of infinite extent.

In the presentation, the required axisymmetric integral equations and kernel functions are first developed from the corresponding three-dimensional theory. In particular, emphasis is placed on the analytical and numerical treatment of the kernels. This is followed by an overview of the numerical implementation, and a demonstration of its merits via the consideration of several examples.

INTRODUCTION

There is a large class of practical engineering problems that involve both axisymmetric geometry and loading. While, in these situations, a full three-dimensional analysis is valid, a reduction in the dimensionality of the problem is often quite beneficial. In the present paper, a boundary element method (BEM) is developed for axisymmetric quasistatic poroelasticity. Unlike the previous work on the subject, this new formulation utilizes the time-dependent fundamental solutions for Biot's consolidation theory and, consequently, involves boundary quantities exclusively. As a result, only the one-dimensional curve, representing the generator of the axisymmetric poroelastic body, needs to be discretized. Of course, this greatly simplifies the task of geometric modelling. Additionally, since the algorithm operates directly in the time domain, very accurate solutions are possible.

The initial application of boundary element methods for axisymmetric bodies includes the indirect formulations of Kermanidis (1975) in elasticity and Jaswon and Symm (1977) in potential flow. Meanwhile, Cruse *et al.* (1977) provided the first direct BEM for axisymmetric elasticity, including both centrifugal and steady-state thermal loading. The latter is equivalent to the examination of steady poroelastic response via the poroelastic–thermoelastic analogy (Terzaghi, 1943). The above boundary element references address generic axisymmetric bodies. The specific problem of the elastic response of piles was examined previously by Butterfield and Banerjee (1971) using an indirect BEM.

Moving next to the realm of quasistatic poroelasticity, Banerjee and Butterfield (1981) discuss a staggered procedure for solving the coupled equations. The algorithm requires solution of the transient pore fluid flow equation followed by a deformation analysis at each time step. This is not a boundary-only formulation, and complete volume discretization is necessary. As an example, the consolidation of a strip foundation was examined. Aramaki and Yasuhara (1985) applied this same scheme for axisymmetric poroelasticity, and examined K_0 and isotropic consolidation of a cylinder. Once again, for their approach, cells are required through the domain.

More recently, the present authors have developed time-domain boundary element formulations for both two- and three-dimensional problems of poroelasticity (Dargush and Banerjee, 1989a), which eliminate the need for volume discretization. These formulations are based upon the fundamental solutions of Nowacki (1966), Cleary (1977) and Rudnicki (1987). Meanwhile, the corresponding coupled thermoelastic BEM is provided in Dargush and Banerjee (1989b, 1990), along with a summary of the well-known analogy. The present

work extends these BEM formulations to axisymmetric consolidation, and thus provides the first boundary-only solution for this class of problems.

In the next section, the governing differential and integral equations are presented for general three-dimensional poroelastic bodies. Then, the integral formulation is specialized for the axisymmetric case via a transformation to cylindrical coordinates. The result is an exact integral equation for axisymmetry. However, for practical engineering analysis, approximations must be introduced in order to solve the applicable initial-boundary value problem. The necessary approximations are provided in the section on numerical implementation, which describes the present boundary element method. Finally, several numerical examples are investigated which highlight the attractiveness of the BEM approach.

Indicial notation is used throughout. Thus, summations are implied by repeated indices, commas represent differentiation with respect to spatial coordinates, and a superposed dot denotes a material time derivative.

GOVERNING EQUATIONS IN THREE DIMENSIONS

The differential equations governing three-dimensional consolidation, as developed by Biot (1941), can be written in the following Cartesian form (Dargush and Banerjee, 1989a):

$$(\lambda+\mu)u_{j,ij}+\mu u_{i,jj}-\beta p_{,i}+f_i=0 \tag{1a}$$

$$\kappa p_{,ii}-\left(\frac{\beta^2}{\lambda_u-\lambda}\right)\dot{p}-\beta\dot{u}_{i,i}+\psi=0. \tag{1b}$$

In (1), u_i represents the displacement, p is the excess pore pressure, f_i is the body force per unit volume, and ψ is the time rate of volumetric fluid supply per unit volume. Latin indices vary from one to three. Meanwhile, λ and μ are the drained Lamé elastic constants, λ_u is the undrained elastic modulus, κ is the permeability and

$$\beta=\frac{3}{B}\left(\frac{\lambda_u-\lambda}{3\lambda_u+2\mu}\right) \tag{2a}$$

where B is Skempton's pore pressure coefficient. For media in which both the fluid and solid constituents are incompressible, $\beta=1$. Additionally, the coefficient of consolidation is defined as

$$c_v=\kappa\left(\frac{\lambda_u-\lambda}{\beta^2}\right)\left(\frac{\lambda+2\mu}{\lambda_u+2\mu}\right) \tag{2b}$$

while the drained elastic modulus E, drained Poisson's ratio ν, and undrained Poisson's ratio ν_u are written as

$$E=\frac{\mu(3\lambda+3\mu)}{(\lambda+\mu)} \tag{2c}$$

$$\nu=\frac{\lambda}{2(\lambda+\mu)} \tag{2d}$$

$$\nu_u=\frac{\lambda_u}{2(\lambda_u+\mu)}. \tag{2e}$$

The corresponding integral equations can be developed either by operating directly on (1) or by starting with the poroelastic reciprocal theorem defined by Ionescu-Cazimir (1964). With zero initial conditions and the absence of body forces and sources, both approaches lead to the following integral equations (Dargush and Banerjee, 1989a):

$$c_{\beta\alpha}(\xi)u_\beta(\xi,\tau) = \int_S [g_{\beta\alpha}(X;\xi,\tau) * t_\beta(X) - f_{\beta\alpha}(X;\xi,\tau) * u_\beta(X)]\,\mathrm{d}S(X) \tag{3}$$

in which the concept of generalized displacement (u_β) and traction (t_β) is introduced with pore pressure and mass flux (q) occupying their respective four components. Thus,

$$u_\beta = \{u_1 \quad u_2 \quad u_3 \quad p\}^{\mathrm{T}} \tag{4a}$$

$$t_\beta = \{t_1 \quad t_2 \quad t_3 \quad q\}^{\mathrm{T}}. \tag{4b}$$

All Greek indices in (3) vary from one to four. Additionally, $g_{\beta\alpha}$ and $f_{\beta\alpha}$ represent kernel functions, which are derived from the fundamental solutions of three-dimensional poroelasticity (Nowacki, 1966; Cleary, 1977). These are defined in Dargush (1987) and Dargush and Banerjee (1989a,b, 1990). The integration is conducted over the surface of the body S and over time, from zero to τ, as indicated by the standard symbol (*) for Riemann convolution integrals. Lastly, the tensor $c_{\beta\alpha}$ depends only upon the local geometry at ξ, and reduces to a generalized delta function $\delta_{\beta\alpha}$ for ξ inside S. Notice, in particular, that the displacement and pore pressure are written strictly in terms of boundary quantities, and that domain integrals are not involved. Consequently, the present approach differs substantially from that of Banerjee and Butterfield (1981) and Aramaki and Yasuhara (1985).

As discussed in Dargush and Banerjee (1989a), the kernels $g_{\beta\alpha}$ and $f_{\beta\alpha}$ can be separated into steady-state and transient components. That is,

$$g_{\beta\alpha} = G_{\beta\alpha} + g^{\mathrm{tr}}_{\beta\alpha} \tag{5a}$$

$$f_{\beta\alpha} = F_{\beta\alpha} + f^{\mathrm{tr}}_{\beta\alpha}. \tag{5b}$$

In this form, all the singularities are contained in the steady-state $G_{\beta\alpha}$ and $F_{\beta\alpha}$ components. The remaining transient portion is completely non-singular.

INTEGRAL FORMULATION FOR AXISYMMETRY

For axisymmetric geometry, it is convenient to introduce a cylindrical coordinate system (r,θ,z). In this system, the surface S is formed by the generator C which lies in the r–z plane as shown in Fig. 1.

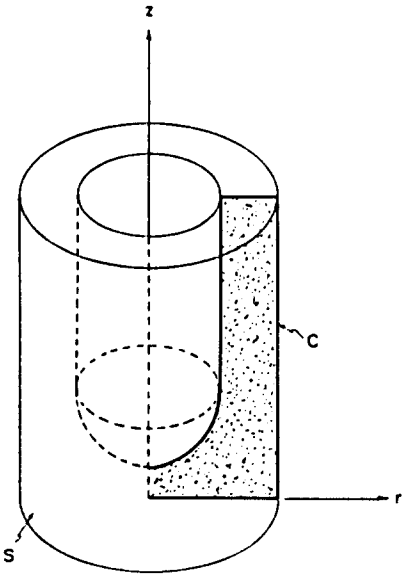

Fig. 1. Axisymmetric geometry.

Transforming the generalized displacements and tractions to this cylindrical system produces

$$\bar{u}_\alpha = T_{\beta\alpha} u_\beta \tag{6a}$$

$$\bar{t}_\alpha = T_{\beta\alpha} t_\beta \tag{6b}$$

where

$$\bar{u}_\alpha = \{u_r \quad u_\theta \quad u_z \quad p\}^T \tag{7a}$$

$$\bar{t}_\alpha = \{t_r \quad t_\theta \quad t_z \quad q\}^T \tag{7b}$$

$$T_{\beta\alpha} = \begin{bmatrix} \cos\theta & -\sin\theta & 0 & 0 \\ \sin\theta & \cos\theta & 0 & 0 \\ 0 & 0 & 1 & 0 \\ 0 & 0 & 0 & 1 \end{bmatrix}. \tag{8}$$

Then, after introducing (5)–(8), the governing integral equations can be rewritten as

$$\bar{c}_{\beta\alpha}(\xi)\bar{u}_\beta(\xi,\tau) = \int_C \int_0^{2\pi} [\bar{G}_{\beta\alpha}(X;\xi)\bar{t}_\beta(X,\tau) - \bar{F}_{\beta\alpha}(X;\xi)\bar{u}_\beta(X,\tau)]\,d\theta\,dC + \int_C \int_0^{2\pi} [\bar{g}^{tr}_{\beta\alpha}(X;\xi,\tau) * \bar{t}_\beta(X) - \bar{f}^{tr}_{\beta\alpha}(X;\xi,\tau) * \bar{u}_\beta(X)]\,d\theta\,dC \tag{9}$$

where

$$\bar{G}_{\beta\alpha} = T_{\gamma\beta} G_{\gamma\delta} \tilde{T}_{\delta\alpha} r \tag{10a}$$

$$\bar{F}_{\beta\alpha} = T_{\gamma\beta} F_{\gamma\delta} \tilde{T}_{\delta\alpha} r \tag{10b}$$

$$\bar{g}^{tr}_{\beta\alpha} = T_{\gamma\beta} g^{tr}_{\gamma\delta} \tilde{T}_{\delta\alpha} r \tag{10c}$$

$$\bar{f}^{tr}_{\beta\alpha} = T_{\gamma\beta} f^{tr}_{\gamma\delta} \tilde{T}_{\delta\alpha} r \tag{10d}$$

$$\bar{c}_{\beta\alpha} = \tilde{T}_{\gamma\beta} c_{\gamma\delta} \tilde{T}_{\delta\alpha}, \tag{10e}$$

with $\tilde{T}_{\delta\alpha}$ representing the transformation in (8) evaluated at ξ.

Restricting the response, to the purely axisymmetric case, eliminates all circumferential variation of the generalized displacements and tractions. In that case, $u_\theta = 0$ and $t_\theta = 0$. As a result, the second degree of freedom can be eliminated from consideration, and (9) can be collapsed to a set of three equations. Thus, the quantities in (9) are redefined such that

$$\bar{u}_\beta = \{u_r \quad u_z \quad p\}^T \tag{11a}$$

$$\bar{t}_\beta = \{t_r \quad t_z \quad q\}^T. \tag{11b}$$

Additionally,

$$\bar{G}_{\beta\alpha} = \begin{bmatrix} \bar{G}_{rr} & \bar{G}_{rz} & \bar{G}_{rp} \\ \bar{G}_{zr} & \bar{G}_{zz} & \bar{G}_{zp} \\ \bar{G}_{pr} & \bar{G}_{pz} & \bar{G}_{pp} \end{bmatrix} \tag{12}$$

with similar notation holding for $\bar{F}_{\beta\alpha}$, $\bar{g}^{tr}_{\beta\alpha}$, $\bar{f}^{tr}_{\beta\alpha}$ and $\bar{c}_{\beta\alpha}$. With this in mind, eqn (9) becomes:

$$\bar{c}_{\beta\alpha}(\xi)\bar{u}_\beta(\xi,\tau) = \int_C [\hat{G}_{\beta\alpha}(X;\xi)\bar{t}_\beta(X,\tau) - \hat{F}_{\beta\alpha}(X;\xi)\bar{u}_\beta(X,\tau)]\,dC$$

$$+ \int_C \int_0^{2\pi} [\bar{g}^{tr}_{\beta\alpha}(X;\xi,\tau) * \bar{t}_\beta(X) - \bar{f}^{tr}_{\beta\alpha}(X;\xi,\tau) * \bar{u}_\beta(X)]\,d\theta\,dC \quad (13)$$

where

$$\hat{G}_{\beta\alpha} = \int_0^{2\pi} \bar{G}_{\beta\alpha}\,d\theta \quad (14a)$$

$$\hat{F}_{\beta\alpha} = \int_0^{2\pi} \bar{F}_{\beta\alpha}\,d\theta. \quad (14b)$$

This circumferential integration in (14) can be evaluated analytically in terms of elliptic integrals for all of the steady-state components. The components $\hat{G}_{rr}$, $\hat{G}_{rz}$, $\hat{G}_{zr}$, $\hat{G}_{zz}$, $\hat{F}_{rr}$, $\hat{F}_{rz}$, $\hat{F}_{zr}$ and $\hat{F}_{zz}$ are identical to those of axisymmetric elasticity. Their explicit form is defined in Henry *et al.* (1987). Meanwhile, $\hat{G}_{pp}$ and $\hat{F}_{pp}$ are the potential flow axisymmetric kernels as presented in Banerjee and Butterfield (1981). The coupling terms $\hat{G}_{pr}$, $\hat{G}_{pz}$, $\hat{F}_{pr}$ and $\hat{F}_{pz}$ are given by Bakr and Fenner (1983) in their formulation for steady-state thermoelasticity. The remaining components for the steady kernels are zero. For reference, the entire $\hat{G}_{\beta\alpha}$ and $\hat{F}_{\beta\alpha}$ kernels are provided in a consistent notation in Dargush (1987) and defined here in Appendix A.

The integral equations (13) are exact statements for axisymmetric quasistatic poroelasticity. However, for the solution of practical problems of soil consolidation, approximations must be introduced. For example, unlike the above treatment for the steady-state components, the circumferential integration of the transient portion of the kernels cannot be expressed in closed form. The numerical treatment of (13) is the subject of the next section.

NUMERICAL IMPLEMENTATION

Details of a numerical algorithm for two and three-dimensional poroelasticity have been given previously by Dargush and Banerjee (1989a). Consequently, this section will focus on those items which are of particular importance to axisymmetry.

The application of (13) for engineering analysis requires discretization and approximation in both time and space. For the temporal representation, the time from zero to τ is subdivided into N equal increments of duration $\Delta\tau$. Within each increment, the primary variables $\bar{u}_\beta$ and $\bar{t}_\beta$ are assumed constant. Thus, during the nth time step, the generalized displacements and tractions are $\bar{u}^n_\beta(X)$ and $\bar{t}^n_\beta(X)$. As a result, the integral equations take the form

$$\bar{c}_{\beta\alpha}(\xi)\bar{u}^N_\beta(\xi) = \int_C [\hat{G}_{\beta\alpha}(X;\xi)\bar{t}^N_\beta(X) - \hat{F}_{\beta\alpha}(X;\xi)\bar{u}^N_\beta(X)]\,dC$$

$$+ \sum_{n=1}^{N} \left\{ \int_C [\hat{G}^{N-n+1}_{\beta\alpha}(X;\xi)\bar{t}^n_\beta(X) - \hat{F}^{N-n+1}_{\beta\alpha}(X;\xi)\bar{u}^n_\beta(X)]\,dC \right\} \quad (15)$$

where

$$\hat{G}_{\beta\alpha}^{N-n+1} = \int_0^{2\pi} \bar{G}_{\beta\alpha}^{N-n+1}\, d\theta \tag{16a}$$

$$\hat{F}_{\beta\alpha}^{N-n+1} = \int_0^{2\pi} \bar{F}_{\beta\alpha}^{N-n+1}\, d\theta \tag{16b}$$

with

$$\bar{G}_{\beta\alpha}^{N-n+1}(X;\xi) = \int_{(n-1)\Delta\tau}^{n\Delta\tau} \bar{g}_{\beta\alpha}^{tr}(X,t;\xi,\tau)\, dt \tag{17a}$$

$$\bar{F}_{\beta\alpha}^{N-n+1}(X;\xi) = \int_{(n-1)\Delta\tau}^{n\Delta\tau} \bar{f}_{\beta\alpha}^{tr}(X,t;\xi,\tau)\, dt. \tag{17b}$$

In light of the transformation (10), eqns (17) can be rewritten as

$$\bar{G}_{\beta\alpha}^{N-n+1} = T_{\gamma\beta} G_{\gamma\delta}^{N-n+1} \tilde{T}_{\delta\alpha} r \tag{18a}$$

$$\bar{F}_{\beta\alpha}^{N-n+1} = T_{\gamma\beta} F_{\gamma\delta}^{N-n+1} \tilde{T}_{\delta\alpha} r \tag{18b}$$

where the Cartesian transient kernels are

$$G_{\gamma\delta}^{N-n+1}(X;\xi) = \int_{(n-1)\Delta\tau}^{n\Delta\tau} g_{\gamma\delta}^{tr}(X,t;\xi,\tau)\, dt \tag{19a}$$

$$F_{\gamma\delta}^{N-n+1}(X;\xi) = \int_{(n-1)\Delta\tau}^{n\Delta\tau} f_{\gamma\delta}^{tr}(X,t;\xi,\tau)\, dt. \tag{19b}$$

The time integration present in (19) can be performed analytically. The resulting transient kernels $G_{\gamma\delta}^{N-n+1}$ and $F_{\gamma\delta}^{N-n+1}$ are provided in Appendix B. These comprise the transient portion of the three-dimensional time-integrated kernels employed in Dargush and Banerjee (1989a). It should be emphasized that $G_{\gamma\delta}^{N-n+1}$ and $F_{\gamma\delta}^{N-n+1}$ are completely non-singular.

Although the integration in (19) is determined analytically, it is not possible to evaluate the circumferential integral of (16) in closed form. Consequently, this integration is performed numerically. Since the kernels involved are non-singular, standard Gauss quadrature formulas are applicable. However, for X in the proximity of ξ, subsegmentation and higher-order Gaussian rules are required to control error. As time progresses, the transient portions of the poroelastic kernels not only diminish in magnitude, but also become more gradual in their spatial variation. In order to take full advantage of this behavior, the present implementation employs adaptive circumferential integration schemes which depend upon the spatial relationship between X and ξ, as well as the time elapsed between t and τ. Eventually, the subsegmentation is eliminated and only a few Gauss points are required even for nearby points.

With the temporal and circumferential integration completely defined, it remains to consider the discretization of C in the r–z plane. For this, the approach taken by Henry *et al.* (1987) is utilized. Three-noded quadratic, conforming surface elements are employed with either linear or quadratic variation of the generalized displacements and tractions. Integration is accomplished numerically through the use of adaptive subsegmentation and Gaussian quadrature. The strongly-singular $\hat{F}_{\beta\alpha}$ kernel components are determined via the indirect rigid body and inflation mode techniques. During the first time step, when $N = 1$, both steady and transient kernels must be integrated. That is, from (15), integration of $\hat{G}_{\beta\alpha}$ and $\hat{G}_{\beta\alpha}^{1}$ is required for multiplication by t_β^1, while $\hat{F}_{\beta\alpha}$ and $\hat{F}_{\beta\alpha}^{1}$ are needed in conjunction with u_β^1. However, for subsequent time steps, only the transient non-singular kernels, $\hat{G}_{\beta\alpha}^{N}$ and $\hat{F}_{\beta\alpha}^{N}$, must be integrated. For example, with $N = 2$, eqn (15) can be written as

$$\bar{c}_{\beta\alpha}(\xi)\bar{u}^2_\beta(\xi) = \int_C [\hat{G}_{\beta\alpha}(X;\xi)\bar{t}^2_\beta(X) - \hat{F}_{\beta\alpha}(X;\xi)\bar{u}^2_\beta(X)]\,dC$$

$$+ \int_C [\hat{G}^1_{\beta\alpha}(X;\xi)\bar{t}^2_\beta(X) - \hat{F}^1_{\beta\alpha}(X;\xi)\bar{u}^2_\beta(X)]\,dC$$

$$+ \int_C [\hat{G}^2_{\beta\alpha}(X;\xi)\bar{t}^1_\beta(X) - \hat{F}^2_{\beta\alpha}(X;\xi)\bar{u}^1_\beta(X)]\,dC. \quad (20)$$

The first four kernels in(20) were already determined during the first time step, as discussed above. Thus, only $\hat{G}^2_{\beta\alpha}$ and $\hat{F}^2_{\beta\alpha}$ require integration.

Collocation provides the basis for the development of the system of governing algebraic equations. Thus, the spatially-discretized version of (15) is written at each boundary node. After imposition of the boundary conditions, the system equations are solved at each time step by invoking a LINPACK-based solver. Afterward, secondary boundary quantities, such as effective stresses, can easily be determined from the constitutive law, along with compatibility relationships.

Since the implementation is accomplished within a general-purpose boundary element code, a number of additional features are readily available for practical engineering analysis. Perhaps the most significant of these items is the ability to analyze substructured problems. This not only permits extension of the formulation to multilayered soils, but often provides computational efficiencies. Another important feature concerns the availability of enclosing elements which were first employed for time-dependent problems by Ahmad and Banerjee (1988). Enclosing elements allow for closure of bodies of infinite extent for the determination of the coefficients corresponding to the strongly-singular integrals. The nodes associated with enclosing elements do not contribute unknowns or equations to the overall system. Furthermore, since the fundamental solutions automatically satisfy the radiation conditions on infinite boundaries, there is no need to introduce artificial boundaries as is typically done in finite element analysis. Other capabilities include symmetry about the r-θ plane, sliding interfaces, time-dependent boundary conditions, and the use of local coordinates. Several of these features are illustrated in the next section, which focuses on the validation of the new poroelastic BEM formulation.

APPLICATIONS

Consolidation of a sphere

As a first example, the classical problem of the consolidation of a sphere is considered. This problem was first solved by Cryer (1963) in terms of an infinite series, and formed the basis of a comparison between the consolidation theories of Biot and Terzaghi.

For the boundary element analysis, the four element model depicted in Fig. 2 was employed. Each element permits quadratic variation of the generalized displacements and tractions. Symmetry about the r-θ plane is assumed. One interior point is also included to monitor response at the center of the sphere.

All dimensions and material properties are normalized to correspond to those used by Cryer. Thus, for example,

$$\mu_c = \frac{\mu}{2\mu+\lambda} \quad (21a)$$

$$\lambda_c = \frac{\lambda}{2\mu+\lambda} \quad (21b)$$

with the subscript c signifying Cryer's notation. Furthermore, let

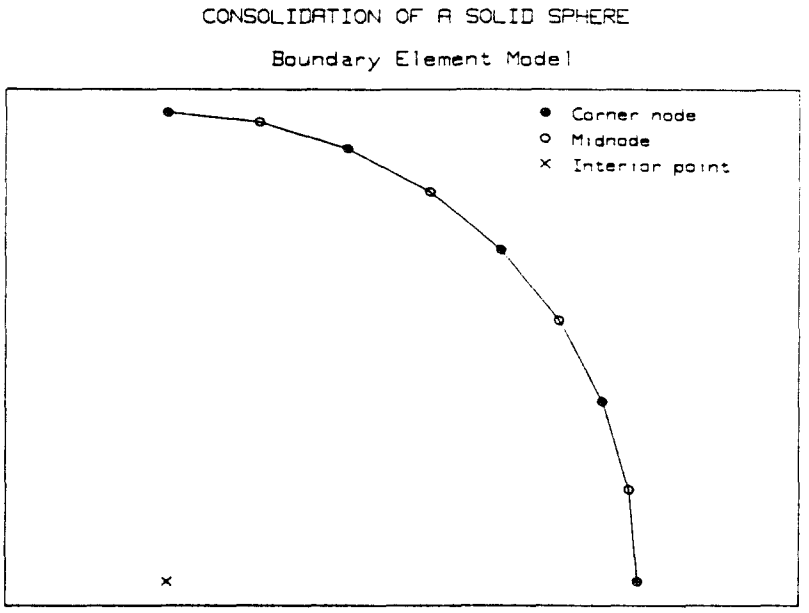

Fig. 2. Consolidation of a sphere—boundary element method.

$$T = \frac{c_v \tau}{a^2} \tag{22a}$$

$$R = \frac{r}{a} \tag{22b}$$

where a is the radius of the sphere. As a result, the radial displacement can be written as $U_R(R, T)$ and the pore pressure as $P(R, T)$.

The boundary element solutions, obtained from the general-purpose computer program GPBEST, are compared to the series of solutions in Figs 3 and 4. Three cases

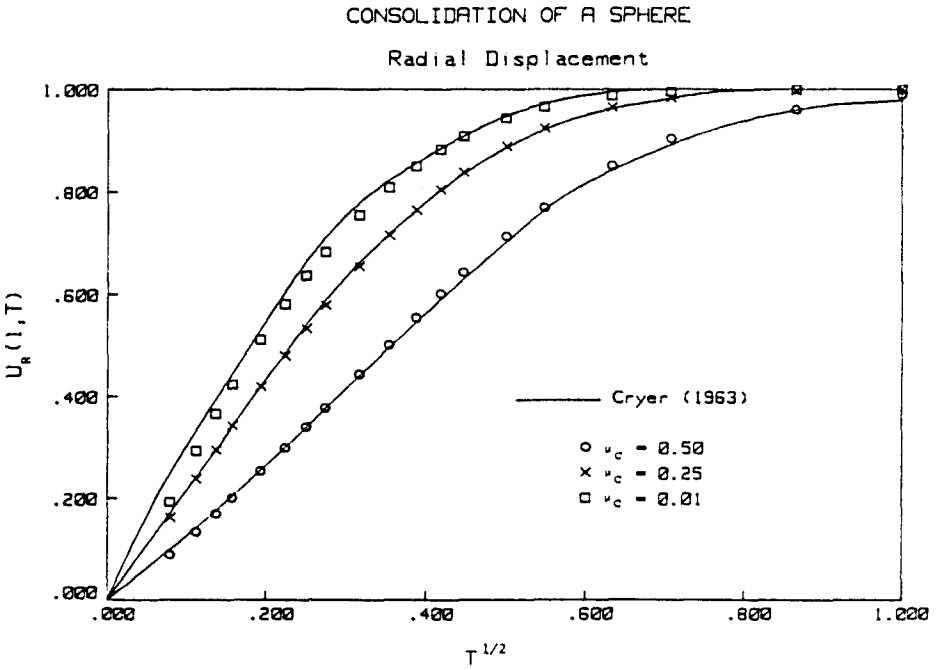

Fig. 3. Consolidation of a sphere—radial displacement.

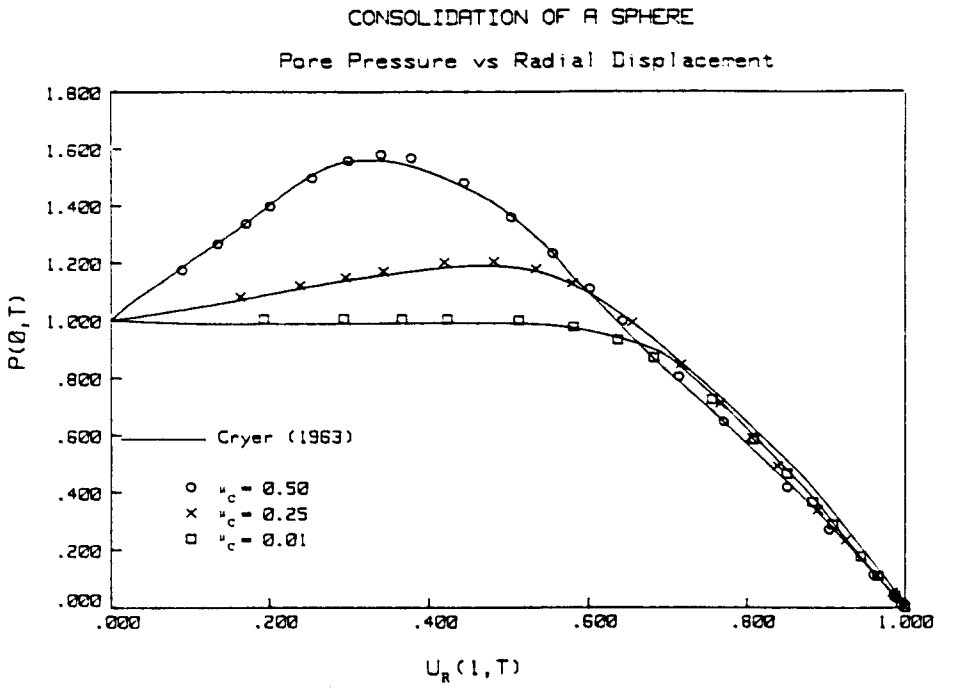

Fig. 4. Consolidation of a sphere—pore pressure vs radial displacement.

($\mu_c = 0.50$, 0.25 and 0.01) are considered. In general, excellent correlation with the results of Cryer is obtained. Notice, in Fig. 4, the initial increase in pore pressure with increasing U_R for $\mu_c = 0.50$ and $\mu_c = 0.25$. This phenomenon is the well-known Mandel–Cryer effect which is present in Biot's theory, but absent for Terzaghi consolidation. For $\mu_c = 0.0$, the governing equations of Biot reduce to those of Terzaghi, such that no Mandel-Cryer effect exists. It is evident from the graphs that the present boundary element formulation accurately reproduces the entire range of this behavior.

Consolidation under a circular load

Analytical solutions are also available for the consolidation of a single poroelastic stratum beneath a uniform vertical circular load. Let H represent the depth of the soil layer and a be the radius of the loaded area. The lower boundary of the soil layer is smooth, but impervious, while free drainage is permitted along the entire upper surface. For comparison non-dimensional forms of the material parameters are utilized. In particular, let $E = 1.0$, $\nu = 0.0$, $\kappa = 1.0$, $\nu_u = 0.5$ and $B = 1.0$. (The diffusivity is unity for this set of properties.)

A uniform traction $t_z = -1.0$ is applied over the circular area suddenly at time zero and then maintained at that level. In this investigation, two cases are considered, $H/a = 1.0$ and 10. Both were examined by Gibson *et al.* (1970), who provided a semi-analytical solution for these axisymmetric problems.

The boundary element mesh employed for the GPBEST analysis is provided in Fig. 5 for $H/a = 10$. Considerable refinement is used near the loaded region. Additionally, notice that the mesh is truncated at a distance $r/a = 40$. Beyond that distance, the upper and lower surfaces have negligible contribution. However, since the rigid body and inflation mode techniques are utilized, several enclosing elements are introduced to ensure the accurate calculation of the strongly-singular diagonal blocks of $\hat{F}_{\beta z}$. A topologically-similar model was also used for the $H/a = 1.0$ case. The boundary element results for the single poroelastic layer are compared with those of Gibson *et al.* in Fig. 6, where the non-dimensional time

$$T = \frac{c_v \tau}{a^2} \tag{23a}$$

and the degree of consolidation

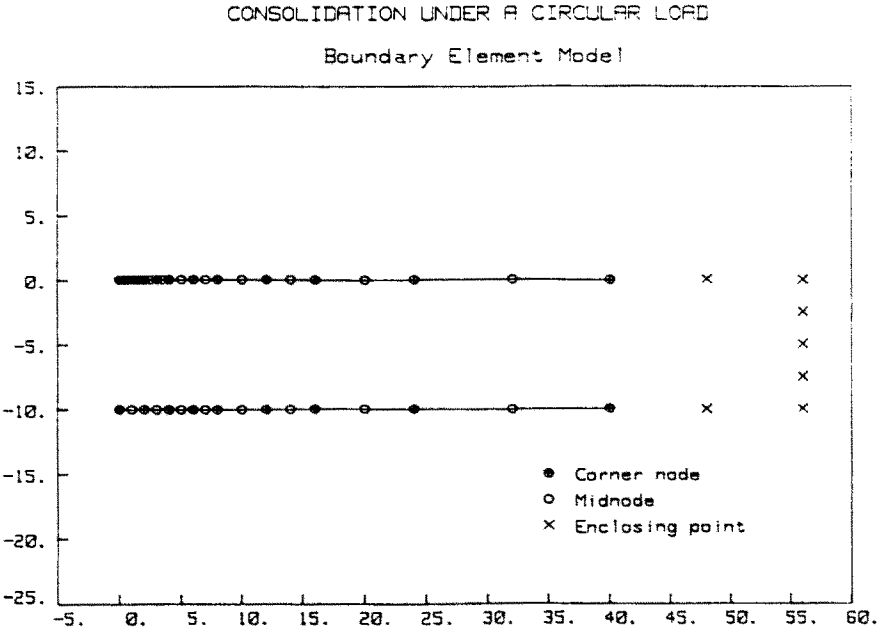

Fig. 5. Consolidation under a circular load—boundary element model.

$$U = \frac{U_z(\tau) - U_z(0)}{U_z(\infty) - U_z(0)} \tag{23b}$$

with $U_z(\tau)$ representing the vertical displacement of the soil at the center of the loaded area at time τ. From the figure, the degree of consolidation correlates very well over the entire process, thus validating the boundary element formulation for bodies of infinite extent.

Multilayer analytical solutions are not available, however the present BEM can be readily applied. For example, consider two soil layers. The upper layer has a depth $H_1 = 2$,

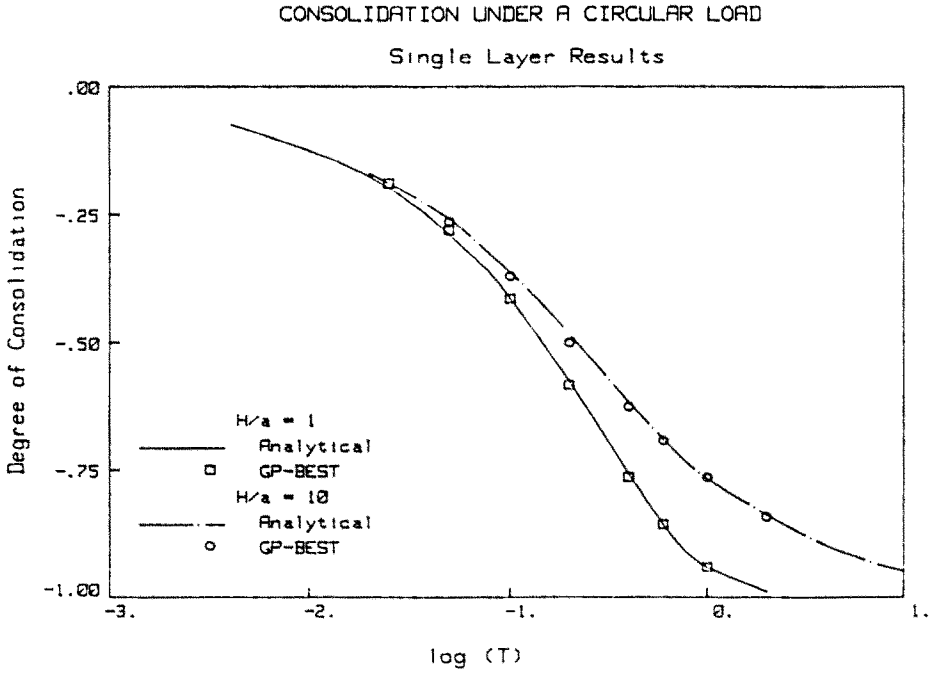

Fig. 6. Consolidation under a circular load—single-layer results.

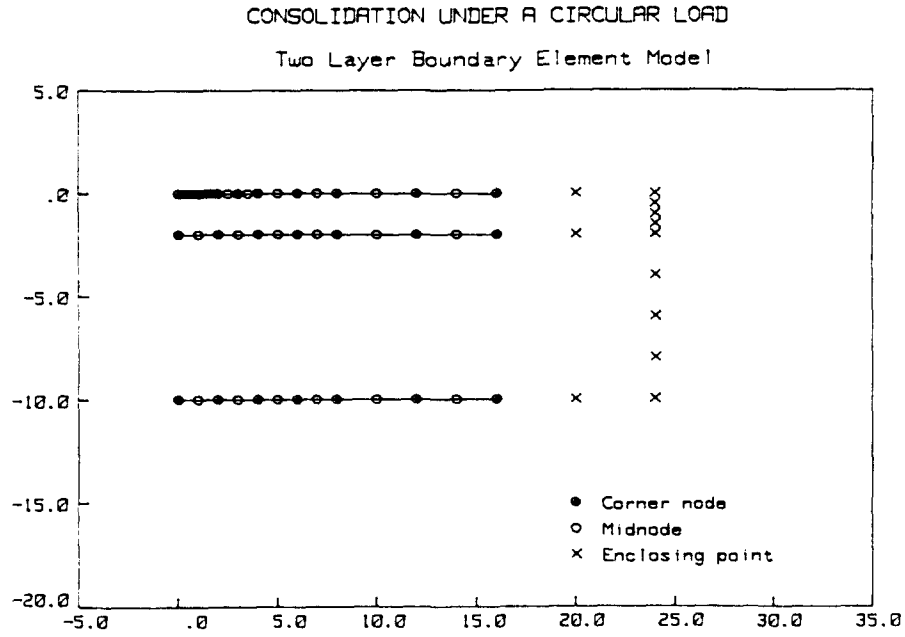

Fig. 7. Consolidation under a circular load—two-layer boundary element model.

while the thickness of the bottom layer is $H_2 = 8$. It is assumed that $E = 1.0$, $\nu = 0.0$, $\nu_u = 0.5$ and $B = 1.0$ for both soils, while the value of the permeability may differ.

The boundary element mesh for the two-layer analysis is shown in Fig. 7, and the results are provided in Fig. 8. Here, the non-dimensional time is with respect to the coefficient of consolidation of the upper layer. As expected, if the lower soil is more permeable, then the consolidation process is expedited. On the other hand, while a less permeable layer retards consolidation, this effect is not as dramatic. Naturally, this analysis could be extended to several additional layers, each with different poroelastic material constants. At this point, it is worth mentioning that since the present BEM formulation utilizes a fully

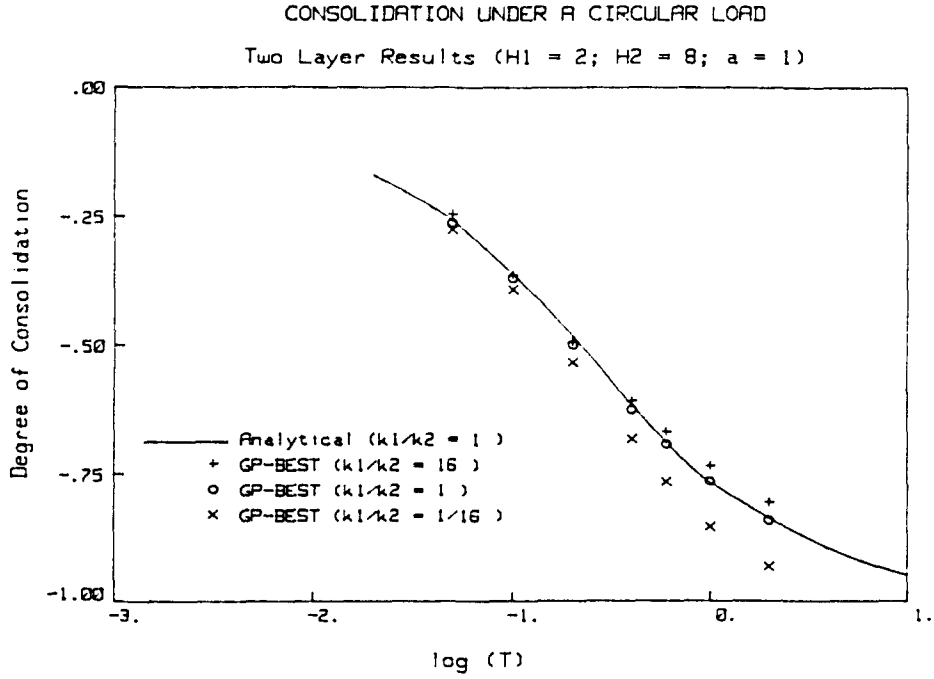

Fig. 8. Consolidation under a circular load—two-layer results.

implicit time-marching scheme, stable numerical results are produced over a wide range of time steps. Thus, the method can handle problems for which the coefficient of consolidation of various layers differs by several orders of magnitude.

Consolidation around a pile

For the final application, consolidation around a vertically-loaded permeable pile is examined. The straight, flat-bottomed, cylindrical pile has a length (L) of 30 ft and a 2 ft diameter (D). The second under-reamed pile, detailed in Fig. 9, was also investigated for comparative purposes. In both cases, the pile is assumed to be fully-saturated concrete with the following poroelastic properties:

$$E = 3.0 \times 10^6 \text{ psi}$$
$$\nu = 0.3$$
$$\nu_u = 0.41$$
$$k = 1.0 \times 10^{-7} \text{ in s}^{-1}$$
$$\gamma_w = 0.036 \text{ lb in}^{-3}$$
$$\kappa = k/\gamma_w.$$

Meanwhile, the surrounding soil, which occupies the remainder of a half-space, is assumed to be a uniform, isotropic clay. The clay properties are taken as:

$$E = 15 \times 10^3 \text{ psi}$$
$$\nu = 0.2$$
$$\nu_u = 0.5$$
$$k = 8.0 \times 10^{-8} \text{ in s}^{-1}$$

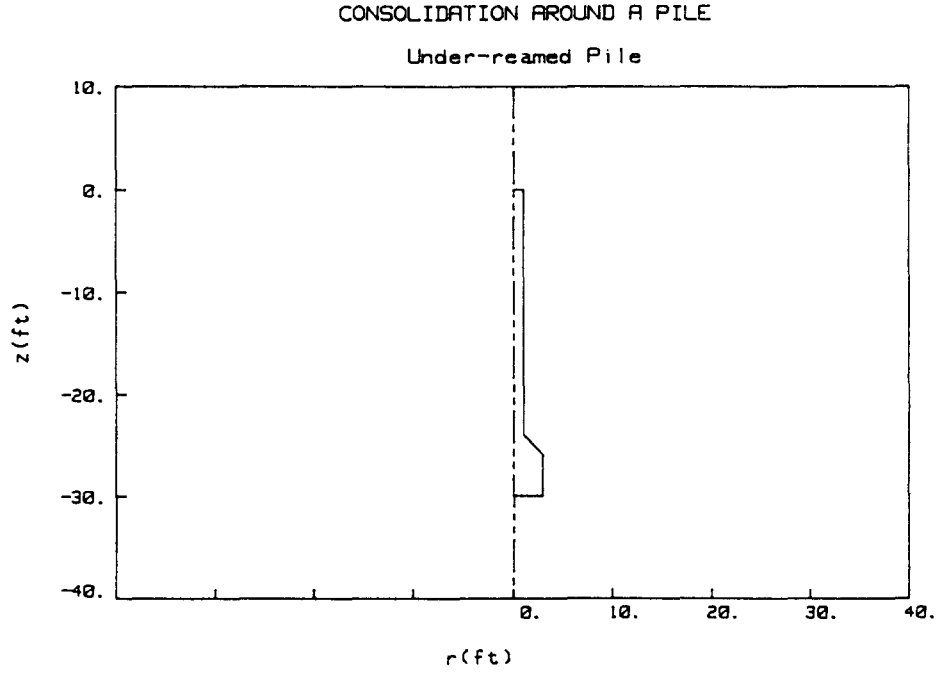

Fig. 9. Consolidation around a pile—under-reamed pile.

$$\gamma_w = 0.036 \text{ lb in}^{-3}.$$

The pile–soil interface is considered fully bonded.

Starting at time zero, a uniform downward vertical traction is continuously applied to the head of the pile. In the boundary element analysis of the ensuing consolidation process, a two-region model is required. The pile model includes refinement near the top and bottom corners. Discretization of the soil is only needed along the pile interface and the half-space surface. Consequently, the modeling required for this problem is minimal. Enclosing elements, once again, permit the finite truncation of the mesh without a significant effect on the solution accuracy.

The consolidation history for the two types of piles is plotted in Fig. 10. In the abscissa, the dimensionless time (T) is determined from the radius of the pile (R) and the coefficient of consolidation of the soil ($c_{v,\text{soil}}$). Thus,

$$T = \frac{c_{v,\text{soil}} t}{R^2}, \tag{24}$$

while the ordinate depicts the degree of consolidation based upon the pile head settlement. Notice that in comparison with Fig. 6, the consolidation around this long narrow object (i.e. the pile) is very slow. For the straight pile only 57% of the process is complete for $T = 133$. The under-reamed pile, having a somewhat bigger base, consolidates slightly faster. However, for both piles the fully-drained settlement is only about 15% greater than the instantaneous undrained response.

Besides settlement, load resistance and interface shear stresses are also of interest. In the straight pile, approximately 4% of the applied axial load is reacted by normal tractions on the base of the pile. The remainder is resisted by shear along the shaft face. The distribution of shear stress along the length of the pile is shown a short time after application

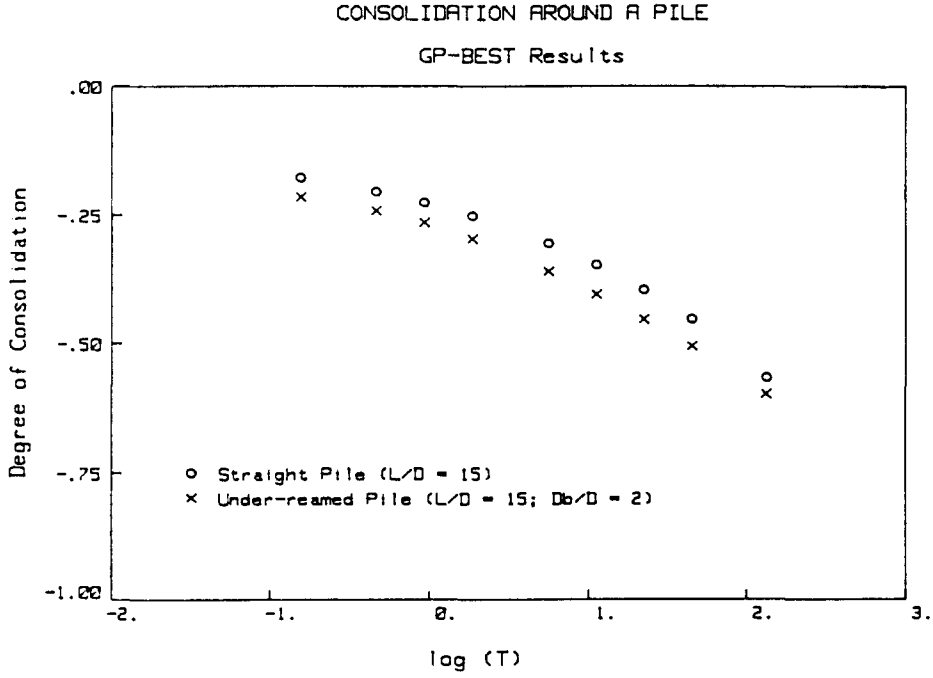

Fig. 10. Consolidation around a pile—degree of consolidation.

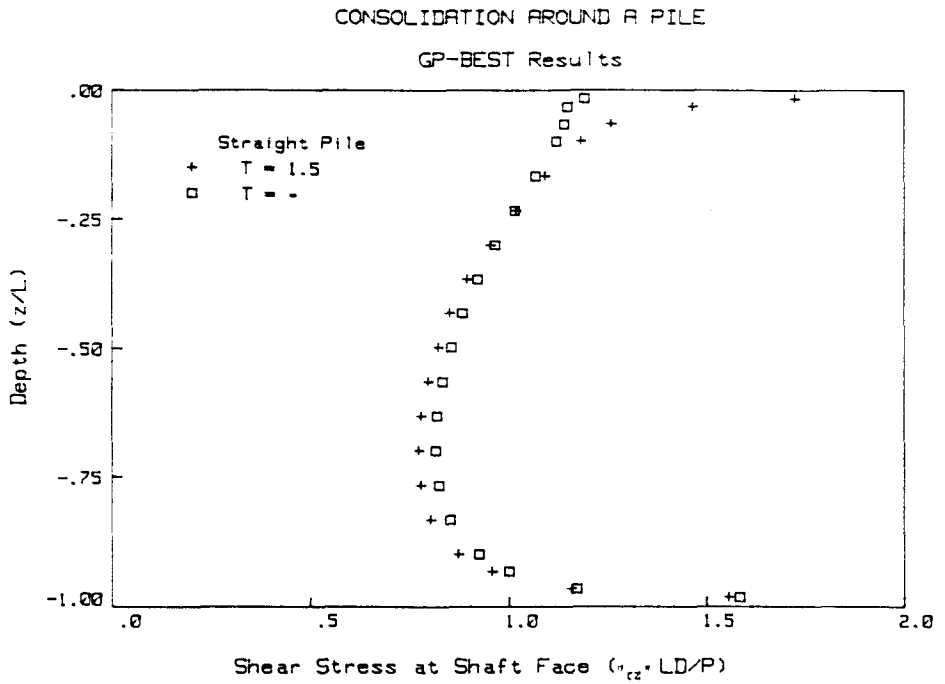

Fig. 11. Consolidation around a pile—shear stress on straight pile.

(i.e. $T = 1.5$) and under drained conditions (i.e. $T = \infty$), in Fig. 11. The drained results are quite similar to those obtained by Butterfield and Banerjee (1971) for moderate L/D compressible piles. However, notice that that short time response includes much higher shear stresses near the surface of the half-space. In Fig. 12, the corresponding results are presented for the under-reamed pile. While the shear stress over much of the length is lower than that for the straight pile, there exists considerable stress concentration in the region of geometric transition. Once again, high shear stress occurs near the surface at short times.

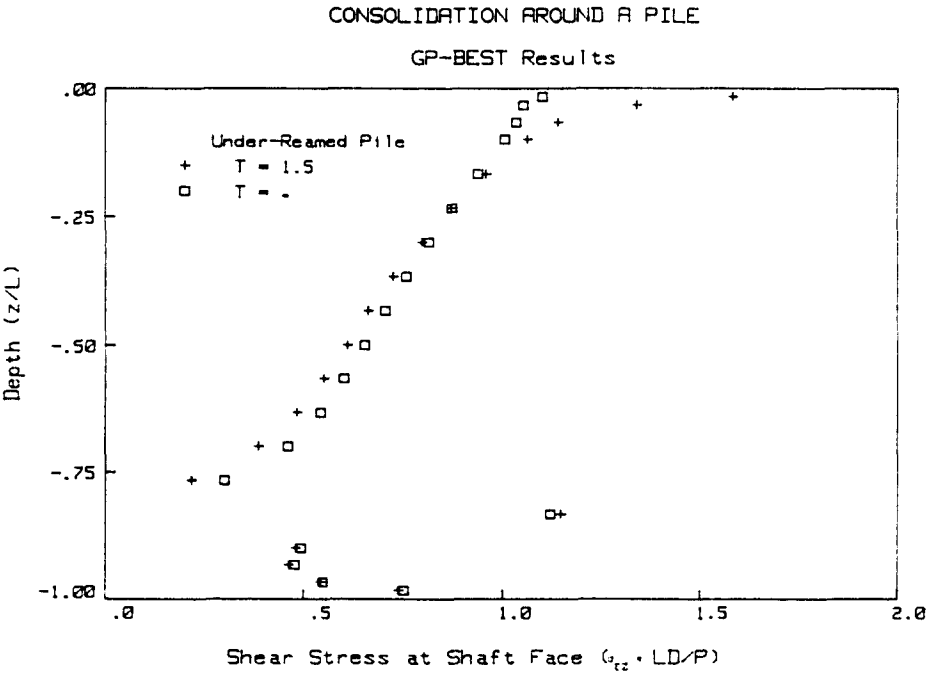

Fig. 12. Consolidation around a pile—shear stress on under-reamed pile.

Finally, it should be noted that the under-reamed pile base reacts approximately 12% of the applied load under drained conditions, and roughly 15% during the initial stages of consolidation.

CONCLUSION

A boundary element method has been developed for axisymmetric problems governed by Biot's consolidation theory. Unlike previous approaches, the present formulation is written directly in the time domain and invokes only boundary quantities. Volume discretization is completely eliminated. Additionally, since the kernel functions satisfy the radiation boundary conditions, there is no need to introduce artificial boundaries or conditions for problems involving regions of infinite extent in one or more spatial dimensions.

In the formulation, the three-dimensional fundamental solution is decomposed into steady-state and transient components. The steady-state components are integrated semi-analytically in the circumferential direction, while the remaining non-singular transient portions are treated numerically.

The entire numerical implementation is accomplished in a general manner, including quadratic elements and multiple regions. Several examples were investigated in detail to emphasize the accuracy and attractiveness of this new BEM.

REFERENCES

Ahmad, S. and Banerjee, P. K. (1988). Transient elastodynamic analysis of three dimensional problems by BEM. *Int. J. Numer. Meth. Engng* **26**, 1560–1580.

Aramaki, G. and Yasuhara, K. (1985). Application of the boundary element method for axisymmetric Biot's consolidation. *Engng Anal.* **2**, 184–191.

Bakr, A. A. and Fenner, R. T. (1983). Boundary integral equation analysis of axisymmetric thermoelastic problems. *J. Strain Anal.* **18**, 239–251.

Banerjee, P. K. and Butterfield, R. (1981). *Boundary Element Methods in Engineering Science*. McGraw-Hill, London.

Biot, M. A. (1941). General theory of three-dimensional consolidation. *J. Appl. Phys.* **12**, 155–164.

Butterfield, R. and Banerjee, P. K. (1971). Elastic analysis of compressible piles and pile groups. *Geotechnique* **21**, 43–60.

Cleary, M. P. (1977). Fundamental solutions for fluid-saturated porous solid. *Int. J. Solids Structures* **13**, 785–806.

Cruse, T. A., Snow, D. W. and Wilson, R. B. (1977). Numerical solutions in axisymmetric elasticity. *Comput. Struct.* **7**, 445–451.

Cryer, C. W. (1963). Comparison of the three-dimensional consolidation theories of Biot and Terzaghi. *Q. J. Mech. Appl. Math.* **16**, 401–412.

Dargush, G. F. (1987). Boundary element methods for the analogous problems of thermomechanics and soil consolidation. Ph.D. Dissertation, State University of New York at Buffalo.

Dargush, G. F. and Banerjee, P. K. (1989a). A time domain boundary element method for poroelasticity. *Int. J. Numer. Meth. Engng* **28**, 2423–2449.

Dargush, G. F. and Banerjee, P. K. (1989b). Boundary element methods for poroelastic and thermoelastic analyses. In *Developments in Boundary Element Methods* (Edited by P. K. Banerjee and R. B. Wilson), Vol. 5, Chapter 4, pp. 119–156. Elsevier, England.

Dargush, G. F. and Banerjee, P. K. (1990). A new BEM formulation for three dimensional problems of consolidation and thermoelasticity. *J. Appl. Mech.* **58**, 28–36.

Gibson, R. E., Schiffman, R. L. and Pu, S. L. (1970). Plane strain and axially symmetric consolidation of a clay layer on a smooth impervious base. *Q. J. Mech. Appl. Math.* **23**, 505–520.

Henry, D. P., Pape, D. A. and Banerjee, P. K. (1987). New axisymmetric BEM formulation for body forces using particular integrals. *J. Engng Mech. ASCE* **113**, 671–688.

Ionescu-Cazimir, V. (1964). Problem of linear coupled thermoelasticity. Theorems on reciprocity for the dynamic problem of coupled thermoelasticity. I. *Bull. l'Acad. Polonaise Sci., Series Sci. Techniques* **12**, 473–488.

Jaswon, M. A. and Symm, G. T. (1977). *Integral Equation Method in Potential Theory and Elastostatics*. Academic Press, London.

Kermanidis, Th. (1975). A numerical solution for axially symmetrical elasticity problems. *Int. J. Solids Structures* **11**, 493–500.

Nowacki, W. (1966). Green's functions for a thermoelastic medium (quasi-static problem). *Bulet. Inst. Polit. Iasi, Serie Noua* **12**(3–4), 83–92.

Rudnicki, J. W. (1987). Fluid mass sources and point forces in linear elastic diffusive solids. *Mech. Mater.* **5**, 383–393.

Terzaghi, K. (1943). *Theoretical Soil Mechanics*. John Wiley, New York.

APPENDIX A: AXISYMMETRIC STEADY-STATE POROELASTIC KERNELS

This Appendix details the generalized boundary kernels for axisymmetric steady-state poroelasticity. These kernels are used in conjunction with numerical tangential integration of the transient portion of the three-dimensional kernels to produce solutions for axisymmetric soil consolidation.

In the following,

$X = x_i = \{R \quad Z\}^T$ coordinates of integration point or ring source.

$\xi = \xi_i = \{r \quad z\}^T$ coordinates of field point.

$n_r(R, Z)$ normal in r direction at integration point.

$n_z(R, Z)$ normal in z direction at integration point.

The indices i, j assume the values 1 and 2 only or, equivalently r and z. Meanwhile, the index p refers to a pore pressure or flux component in the third position of the generalized displacement or traction vector, respectively. Thus, for example, u_p is the pore pressure, while t_p represents the flux. The Greek indices α, β vary from 1 to 3.

Then, for the displacement kernel, let

$$\hat{G}_{\beta\alpha} = A_{\beta\alpha}K(m) + B_{\beta\alpha}E(m)$$

where

$K(m)$ = complete Elliptic Integral of the first kind

$E(m)$ = complete Elliptic Integral of the second kind

$$A_{rr} = \frac{a_1}{rRH}(b_1 M + \bar{Z}^2) \qquad B_{rr} = -\frac{a_1}{rRH}\left(b_1 H^2 + \frac{M\bar{Z}^2}{\rho^2}\right)$$

$$A_{rz} = \frac{a_1 \bar{Z}}{RH} \qquad B_{rz} = -\frac{a_1 \bar{Z}}{R\rho^2 H}\bar{H}$$

$$A_{zr} = -\frac{a_1 \bar{Z}}{rH} \qquad B_{zr} = \frac{a_1 \bar{Z}}{r\rho^2 H}N$$

$$A_{zz} = \frac{2a_1}{H}b_1 \qquad B_{zz} = \frac{2a_1 \bar{Z}^2}{\rho^2 H}$$

$$A_{rp} = 0 \qquad B_{rp} = 0$$

$$A_{zp} = 0 \qquad B_{zp} = 0$$

$$A_{pr} = \frac{a_2 N}{rH} \qquad B_{pr} = -\frac{a_2 H}{r}$$

$$A_{pz} = \frac{2a_2 \bar{Z}}{H} \qquad B_{pz} = 0$$

$$A_{pp} = \frac{2a_1}{H} \qquad B_{pp} = 0$$

$$\bar{Z} = Z - z$$

$$H^2 = (R+r)^2 + \bar{Z}^2$$

$$\rho^2 = [(R-r)^2 + \bar{Z}^2]$$

$$M = R^2 + r^2 + \bar{Z}^2$$

$$N = R^2 - r^2 + \bar{Z}^2$$

$$\bar{H} = R^2 - r^2 - \bar{Z}^2$$

$$m = \frac{4Rr}{H^2}$$

$$a_1 = \frac{R}{8\pi\mu(1-\nu)} \qquad b_1 = (3-4\nu)$$

$$a_2 = \frac{R\beta}{4\pi\kappa(\lambda+2\mu)}$$

$$a_3 = \frac{R}{2\pi\kappa}.$$

While, for the traction kernel,

$$\hat{F}_{rr} = \frac{2\mu}{(1-2\nu)}\left[(1-\nu)\frac{\partial \hat{G}_{rr}}{\partial R} + \nu\left(\frac{\hat{G}_{rr}}{R} + \frac{\partial \hat{G}_{zr}}{\partial Z}\right)\right]n_r + \mu\left[\frac{\partial \hat{G}_{rr}}{\partial Z} + \frac{\partial \hat{G}_{zr}}{\partial R}\right]n_z$$

$$\hat{F}_{zr} = \frac{2\mu}{(1-2\nu)}\left[(1-\nu)\frac{\partial \hat{G}_{zr}}{\partial Z} + \nu\left(\frac{\hat{G}_{rr}}{R} + \frac{\partial \hat{G}_{rr}}{\partial R}\right)\right]n_z + \mu\left[\frac{\partial \hat{G}_{rr}}{\partial Z} + \frac{\partial \hat{G}_{zr}}{\partial R}\right]n_r$$

$$\hat{F}_{r\theta} = 0 \quad \hat{F}_{z\theta} = 0$$

$$\hat{F}_{pr} = \left[\left(\frac{r^2+R^2}{rRH}\right)a_2\kappa K(m) + \left(\frac{M\bar{Z}^2}{rRH\rho^2} - \frac{H}{rR}\right)a_2\kappa E(m)\right]n_r + \left[\left(\frac{\bar{Z}}{rH}\right)a_2\kappa K(m) - \left(\frac{N\bar{Z}}{rH\rho^2}\right)a_2\kappa E(m)\right]n_z$$

$$\hat{F}_{pz} = \left[-\left(\frac{\bar{Z}}{RH}\right)a_2\kappa K(m) - \left(\frac{A\bar{Z}}{RH\rho^2}\right)a_2\kappa E(m)\right]n_r + \left[\left(\frac{2}{H}\right)a_2\kappa K(m) - \left(\frac{2\bar{Z}^2}{H\rho^2}\right)E(m)\right]n_z$$

$$\hat{F}_{p\theta} = \left[\left(\frac{1}{RH}\right)a_3\kappa K(m) + \left(\frac{2(R-r)}{\rho^2 H} - \frac{1}{RH}\right)a_3\kappa E(m)\right]n_r + \left[\left(\frac{2\bar{Z}}{\rho^2 H}\right)E(m)\right]n_z$$

where

$$\frac{\partial \hat{G}_{ij}}{\partial R} = \frac{\partial A_{ij}}{\partial R}K + \frac{\partial B_{ij}}{\partial R}E + A_{ij}\frac{\partial K}{\partial R} + B_{ij}\frac{\partial E}{\partial R}$$

$$\frac{\partial \hat{G}_{ij}}{\partial Z} = \frac{\partial A_{ij}}{\partial Z}K + \frac{\partial B_{ij}}{\partial Z}E + A_{ij}\frac{\partial K}{\partial Z} + B_{ij}\frac{\partial E}{\partial Z}$$

$$\frac{\partial A_{rr}}{\partial R} = \frac{2a_1b_1}{rH} - d_1A_{rr} \qquad \frac{\partial B_{rr}}{\partial R} = -\frac{2a_1s_1}{RrH} - d_1B_{rr}$$

$$\frac{\partial A_{rz}}{\partial R} = -d_1A_{rz} \qquad \frac{\partial B_{rz}}{\partial R} = \frac{2a_1\bar{Z}}{\rho^2 H} - \left(\frac{1}{R} + d_2\right)B_{rz}$$

$$\frac{\partial A_{zr}}{\partial R} = -p_1A_{zr} \qquad \frac{\partial B_{zr}}{\partial R} = \frac{2a_1R\bar{Z}}{r\rho^2 H} - d_2B_{zr}$$

$$\frac{\partial A_{zz}}{\partial R} = -p_1A_{zz} \qquad \frac{\partial B_{zz}}{\partial R} = -d_2B_{zz}$$

$$\frac{\partial A_{rr}}{\partial Z} = \frac{a_1 8(1-\nu)\bar{Z}}{rRH} - \frac{\bar{Z}}{A^2}A_{rr} \qquad \frac{\partial B_{rr}}{\partial Z} = -\frac{2a_1\bar{Z}}{RrH}s_2 - \frac{\bar{Z}}{H^2}B_{rr}$$

$$\frac{\partial A_{rz}}{\partial Z} = \frac{a_1}{RH} - \frac{\bar{Z}}{H^2}A_{rz} \qquad \frac{\partial B_{rz}}{\partial Z} = \frac{a_1}{R\rho^2 H}d_4 - d_3B_{rz}$$

$$\frac{\partial A_{zr}}{\partial Z} = -\frac{a_1}{rH} - \frac{\bar{Z}}{H^2}A_{zr} \qquad \frac{\partial B_{zr}}{\partial Z} = \frac{a_1}{r\rho^2 H}d_5 - d_3B_{zr}$$

$$\frac{\partial A_{zz}}{\partial Z} = -\frac{\bar{Z}}{H^2}A_{zz} \qquad \frac{\partial B_{zz}}{\partial Z} = \frac{4a_1\bar{Z}}{\rho^2 H} - d_3B_{zz}$$

$$p_1 = \frac{R+r}{H^2}$$

$$d_1 = \frac{1}{R} + p_1$$

$$d_2 = p_1 + \frac{2(R-r)}{\rho^2}$$

$$d_3 = \bar{Z}\left(\frac{2}{\rho^2} + \frac{1}{H^2}\right)$$

$$d_4 = N - 4\bar{Z}^2$$

$$d_5 = N + 2\bar{Z}^2$$

$$s_1 = b_1(R+r) + \frac{\bar{Z}^2 r}{\rho^4}(M - 2R^2)$$

$$s_2 = b_1 - \frac{2\bar{Z}^2 Rr}{\rho^4} + \frac{M}{\rho^2}$$

$$\frac{\partial K}{\partial R} = \frac{(M-2R^2)P}{2R} \qquad \frac{\partial E}{\partial R} = -\frac{(M-2R^2)Q}{2RH^2}$$

$$\frac{\partial K}{\partial Z} = -\bar{Z}P \qquad \frac{\partial E}{\partial Z} = \frac{\bar{Z}}{H^2}Q$$

$$P = \frac{E}{\rho^2} - \frac{K}{H^2} \qquad Q = K - E.$$

APPENDIX B: THREE-DIMENSIONAL TRANSIENT POROELASTIC KERNELS

This appendix contains the detailed presentations of all the transient kernel functions utilized in the poroelastic boundary element formulation. These three-dimensional kernels are based upon continuous source and force fundamental solutions. As a result, the following relationships must be used to determine the proper form of the functions required in the boundary element discretization. That is,

$$G^n_{\beta\alpha}(X;\xi) = G_{\beta\alpha}(X;\xi,n\Delta\tau) \qquad \text{for} \quad n = 1$$

$$G^n_{\beta\alpha}(X;\xi) = G_{\beta\alpha}(X;\xi,n\Delta\tau) - G_{\beta\alpha}(X;\xi,(n-1)\Delta\tau) \qquad \text{for} \quad n > 1,$$

with similar expressions holding for the remaining kernels. In the specification of these kernels below, the arguments $(X;\xi,\tau)$ are assumed.

The indices

i, j, k, l vary from 1 to 3

α, β vary from 1 to 4

p equals 4.

Additionally,

x_i coordinates of integration point

ξ_i coordinates of field point

$$y_i = x_i - \xi_i$$

$$r^2 = y_i y_i$$

$$\eta = \frac{r}{(c_t\tau)^{1/2}}$$

$$c_t = \frac{v_u - v}{1 - v_u}.$$

For the generalized transient displacement kernel,

$$G_{ij} = \frac{1}{16\pi r}\frac{1}{\mu(1-v)}\left[\left(\frac{y_i y_j}{r^2}\right)g_1(\eta) + (\delta_{ij})g_2(\eta)\right]$$

$$G_{ip} = \frac{1}{4\pi}\left(\frac{\beta}{\kappa(\lambda+2\mu)}\right)\left[\left(\frac{y_i}{r}\right)g_3(\eta)\right]$$

$$G_{pj} = \frac{1}{8\pi}\left(\frac{\beta}{\kappa(\lambda+2\mu)}\right)\left[\left(\frac{y_j}{r}\right)g_4(\eta)\right]$$

$$G_{pp} = \frac{1}{4\pi r}\left(\frac{1}{\kappa}\right)[g_5(\eta)]$$

whereas, for the generalized transient traction kernel,

$$F_{ij} = \frac{1}{8\pi r^2}\frac{1}{1-v}\left[-\left(\frac{y_i y_j y_k n_k}{r^2}\right)f_1(\eta) - \left(\frac{\delta_{ij}y_k n_k + y_i n_j}{r}\right)f_2(\eta) + \left(\frac{y_i n_j}{r}\right)f_3(\eta)\right]$$

$$F_{ip} = \frac{1}{2\pi r}\left(\frac{\mu\beta}{\kappa(\lambda+2\mu)}\right)\left[\left(\frac{y_i y_k n_k}{r^2}\right)f_4(\eta) + (n_i)f_5(\eta)\right]$$

$$F_{pj} = \frac{1}{8\pi r}\left(\frac{\beta}{\lambda+2\mu}\right)\left[\left(\frac{y_j y_k n_k}{r^2}\right)f_6(\eta) - (n_j)f_7(\eta)\right]$$

$$F_{pp} = \frac{1}{4\pi r^2}\left[\left(\frac{y_k n_k}{r}\right)f_8(\eta)\right].$$

In the above,

$$\operatorname{erf}(z) = \frac{2}{\sqrt{\pi}}\int_0^z e^{-x^2}\,dx$$

$$h_1(\eta) = \operatorname{erf}\left(\frac{\eta}{2}\right) - \frac{\eta}{\sqrt{\pi}}e^{-\eta^2/4} \quad h_1' = \frac{\partial h_1}{\partial \eta}$$

$$h_2(\eta) = \frac{6h_1(\eta)}{\eta^2} - \frac{\eta}{\sqrt{\pi}}e^{-\eta^2/4}$$

$$g_1(\eta) = c_1\{h_1(\eta) - h_2(\eta)\}$$

$$g_2(\eta) = -c_1\left\{h_1(\eta) - \frac{h_2(\eta)}{3} + \frac{2\eta}{3\sqrt{\pi}}e^{-\eta^2/4}\right\}$$

$$g_3(\eta) = \frac{h_1(\eta)}{\eta^2 t}$$

$$g_4(\eta) = -\operatorname{erf}\left(\frac{\eta}{2}\right) + \frac{2h_1(\eta)}{\eta^2}$$

$$g_5(\eta) = -\operatorname{erf}\left(\frac{\eta}{2}\right)$$

$$f_1(\eta) = 3c_1\left\{h_1 - \frac{5h_2}{3}\right\}$$

$$f_2(\eta) = -c_1\{h_1 - h_2\}$$

$$f_3(\eta) = c_1\{h_1 + h_2\}$$

$$f_4(\eta) = \frac{h_1'}{\eta t} - \frac{3h_1}{\eta^2 t}$$

$$f_5(\eta) = \frac{h_1(\eta)}{\eta^2 t} - \frac{h_1'}{\eta t}$$

$$f_6(\eta) = -\operatorname{erf}\left(\frac{\eta}{2}\right) + \frac{6h_1(\eta)}{\eta^2}$$

$$f_7(\eta) = -\operatorname{erf}\left(\frac{\eta}{2}\right) + \frac{2h_1(\eta)}{\eta^2}$$

$$f_8(\eta) = -h_1(\eta).$$